Trans-scale spatial variability of lime-cement mixed columns

Construction and Building Materials 417 (2024) 135394

Contents lists available at ScienceDirect

Construction and Building Materials

journal homepage: www.elsevier.com/locate/conbuildmat

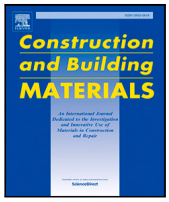

Trans-scale spatial variability of lime-cement mixed columns

Dawn Yun-Cheng Wong [a,*], Vijayshree Sadasivan [a], Jonatan Isaksson [a,b], Anders Karlsson [a], Jelke Dijkstra [a]

[a] Chalmers University of Technology, Department of Architecture and Civil Engineering, Gothenburg, SE-412 96, Sweden
[b] NCC Infrastructure, NCC Sverige AB, Gothenburg, SE 412 50, Sweden

ARTICLE INFO

Keywords:
Spatial variability
Deep mixing
Cement-stabilised soils
Lime-cement columns
Scale of fluctuation
X-ray tomography

ABSTRACT

Lime-cement columns are a common form of ground improvement used in the Nordic countries to improve the engineering properties of soft soils. The strength and stiffness of lime-cement mixed clay, however, are heterogeneous. Hence, the characterisation of the extent of variability of strength and stiffness is essential to optimise the performance of lime-cement columns. This paper presents an integrated approach to characterise the variability in strength and stiffness of samples from 1 year old lime-cement columns in natural sensitive clay, from the Centralen project site in Gothenburg, Sweden. A novel image-based method is proposed to characterise the spatial variability at the laboratory scale, using a stereoscopic digital image correlation (DIC) system in addition to X-ray Computed Tomography (XCT) scans. Data from column penetration tests (FKPS) and reverse column penetration tests (FOPS) on the lime-cement columns at the excavation site were used to estimate the spatial variability at the field scale. The key finding of this work is that different magnitudes of scales of fluctuations exist for the lime-cement mixed clay under laboratory scale and field scale testing. The results serve to highlight the ever-present problem of inherent variability in lime-cement mixed soils and challenges to accurately characterise this variability. Thus, further work is required to relate scale of fluctuation of strength to that of stiffness, and to link scale of fluctuation at laboratory scale with that at field scale.

1. Introduction

Deep mixing (DM) is an in-situ method that improves the engineering properties of soft soils [1–3]. One of those methods is the dry deep mixing method, in which dry binders, often lime and cement, are injected and mixed in the soft clayey soil using compressed air to form lime-cement columns. In Sweden, lime-cement columns are commonly used to increase the stability and to control deformations of various geostructures in soft soils, such as the foundation of railway embankments or basal reinforcement of deep excavations.

In Swedish practice, the shear strength typically governs the design of lime-cement columns [4]. The engineering properties of improved soil are directly affected by the binder, properties of the soil, and mixing and curing conditions [2,5–10]. In addition, the mineral properties of the soft soil (clay) and the binders also affect the response [11]. Finally, the type of loading path further complicates the strength interpretation from laboratory tests [12]. In the design of foundations for railway infrastructure, where the control of vibrations and settlements are more important than the ultimate load, stiffness is the more pertinent requirement than strength. There are far fewer studies that investigate the stiffness properties of lime-cement mixed clay. In the Swedish standard, an empirical relation relating Young's modulus and critical shear strength of the lime-cement composite is used, up to a maximum shear strength of 150 kPa [4].

The strength and stiffness of the lime-cement mixed clay is often highly variable due variation in geology and the complex mixing process. From field tests on installation techniques of lime-cement columns, Larsson et al. [6] found that the blade rotation number, which is a function of the number of mixing blades on the mixing tool and the retrieval rate and rotation speed, has a significant influence on the stabilisation effect and mixing quality. Moreover, the behaviour of a dry binder and soil mixture is complex, and the distribution of the dry binder particles during the deep mixing process is influenced by the viscoelastic properties of the soil [13]. Consequently, the strength is highly variable in magnitude and spatial distribution even if the installation is performed with great care [6]. Aside from inherent variability, additional sources of geotechnical uncertainty include measurement error and transformation uncertainty. The former is caused by equipment, procedural-operator effects, and random testing effects while the latter is introduced when field or laboratory measurements are transformed into design soil properties using empirical or other correlation models [14].

* Corresponding author.
E-mail address: dawn.wong@chalmers.se (D.Y.-C. Wong).

https://doi.org/10.1016/j.conbuildmat.2024.135394
Received 6 October 2023; Received in revised form 5 February 2024; Accepted 7 February 2024
Available online 10 February 2024

Horpibulsuk et al. [15] reported that for a given water-to-cement ratio, most field strength is lower than laboratory strength for dry mixing method, for all curing times, likely due to non-uniformity in mixing [16]. Comparing field cores and laboratory-mixed samples, Madhyannapu et al. [17] found that both field stiffness and strength are 20 to 40 percent lower than the corresponding laboratory-mixed samples. For the case of lime-cement improved soils by the dry deep mixing method, Puppala et al. [18] reported that both field stiffness and strength are lower than the laboratory-mixed samples due to variation in mixing quality over large areas of treatment. However, Paniagua et al. [19] reported an opposite trend of a higher strength, and consequently stiffness, in the field due to a combined effect of higher curing temperatures, and stresses acting on the lime-cement column during curing. These findings highlight the difficulty in accurately characterising the strength and stiffness properties of improved soils in the field, which is a result of the combination of the inherent variability of the site and the variability introduced during the mixing process.

High variability, with respect to the magnitude of the engineering properties and their spatial distribution, introduces uncertainty when estimating the properties of improved soil. In vibration problems, Coelho et al. [20] demonstrated that the maximum vibration level is consistently underestimated when spatial variability is neglected, which can lead to vibration related serviceability issues. Thus it is important to evaluate the influence of variability of both the strength and stiffness on the performance of the lime-cement columns. Aside from the mean and standard deviation, the scale of fluctuation (SOF) is a measure for describing the spatial variation of the (engineered) soil property [21,22]. The spatial variability of shear strength has been studied in natural soils (e.g. [23,24]) and for soils improved with the wet deep mixing method [8,25–28]. In contrast, there are far fewer studies on lime-cement mixed clays [29–31].

Two techniques are commonly employed to characterise field variability of strength in improved soils, firstly coring at various depths and locations to obtain samples for testing [8,25,27], and the use of column penetration tests to obtain a continuous distribution of shear strength with depth for each column [6,29]. The latter gives a better representation of the variability with depth, but can only be done on young columns with low strength. Another limitation of these methods is the time and resources required for testing at field scale.

This paper presents an integrated approach to estimate the spatial variability in lime-cement columns at field and laboratory scale, using samples and quality control data obtained from an excavation site located in Gothenburg, Sweden. At the laboratory scale, stereoscopic observations of surface deformations during an Unconfined Compression Strength (UCS) test were combined with X-ray Computed Tomography (XCT) scans of specimens, to estimate the scale of fluctuation of field-mixed samples. Additionally, the scale of fluctuation of shear strength in the field was estimated from column penetration and reverse column penetration test data. Evaluating the spatial variability of stiffness in the field poses a challenge as there are no direct measures of the variation of stiffness available on site. Thus, unconfined compression tests on 1-year cured samples were used to relate strength and stiffness.

The results of these studies demonstrate the feasibility of the integrated approach to characterise different aspects of variability in lime-cement mixed soils. While the different methods proposed in this work result in different estimates of the variability in strength and stiffness, both at the laboratory scale and in the field, the findings still provide valuable insight on the degree of variability in lime-cement mixed soils and highlight the challenges involved in characterising this variability.

2. Site description

The data presented in this study was obtained from an excavation, which is part of Gothenburg Central Station (Centralen) site in the West Link railway construction project (Fig. 1(a)). The section reported herein comprises a 200 m long braced excavation and was supported by sheet-pile walls, lime-cement columns, and two levels of struts. The passive side of the excavation was stabilised by lime-cement columns constructed in a double overlap rectangular grid pattern with 2.5 m spacing (Fig. 2). The lime-cement content used above and below the excavation level were 40 kg m^{-3} and 80 kg m^{-3}, respectively [32]. A comprehensive site investigation was conducted to characterise the properties of the soft natural clay and lime-cement columns in the site by the Swedish Transportation Administration [33]. The site consists of a 2 m to 5 m thick layer of fill underlain by a deep clay deposit. The groundwater level is located at a depth of 2 m to 3 m with some seasonal fluctuations. The clay deposit is classified as medium sensitive and layers are normally consolidated to slightly overconsolidated with an undrained shear strength ranging from 26 kPa to 60 kPa [32].

3. Methods

3.1. Field tests

3.1.1. Column penetration test

The predrilled column penetration test (FKPS) is a cylindrical penetrometer with two horizontal vanes. For the majority of the tests a probe with dimensions 500 mm × 15 mm was used to test the lime-cement columns of 700 mm diameter. In cases where an overly high strength was encountered, a smaller probe with dimensions 250 mm × 15 mm was used. A pilot hole with a diameter of 58 mm was drilled into each lime-cement column before the FKPS probe was pushed vertically into the lime-cement column at a constant rate of penetration of 20 mm s^{-1} and the penetration resistance was recorded every 20 mm. The test is terminated when the target depth is reached (bottom of the column) or the inclination of the probe deviates out of the acceptable range. The (undrained) shear strength (s_u) was determined from the penetration resistance $q_{c,FKPS}$ with an empirical cone factor $N_{k,FKPS}$ = 10 [4]:

$$s_u = \frac{q_{c,FKPS}}{N_{k,FKPS}} \tag{1}$$

Thenceforth, the strength evaluated from the column penetration tests will be referred to as the shear strength of the lime-cement mixed clay, due to the ambiguity of the drainage condition during the test.

The FKPS data presented in this study were obtained from tests conducted 5 to 10 days after construction of the lime-cement column. A total of 202 tests were used to estimate the spatial variability of the site.

3.1.2. Reverse column penetration test

The FOPS is performed by pulling a pre-installed probe, similar to the probe in the FKPS, upwards from the base of the lime-cement column. The probe with an attached steel wire is installed at the target depth before the construction of the column. The total pull-out force to pull the probe from the base of the column to the surface, including the steel wire friction, was recorded every 25 mm.

The FOPS data presented in this study was obtained from tests conducted 1 to 5 days after construction of the lime-cement column and a total of 29 data sets were used to estimate the spatial variability of the test columns at the site. The locations of the FKPS and FOPS tests conducted are shown in Fig. 1(b).

3.2. Laboratory tests

3.2.1. Sample preparation

Block samples of the lime-cement columns were obtained from the excavated material from the Gothenburg Central Station site. The block samples were excavated from a depth of approximately 5 m to 7 m (low binder content of 40 kg m^{-3}, Fig. 2) for further laboratory testing. The curing period of the samples was approximately 1 year at the

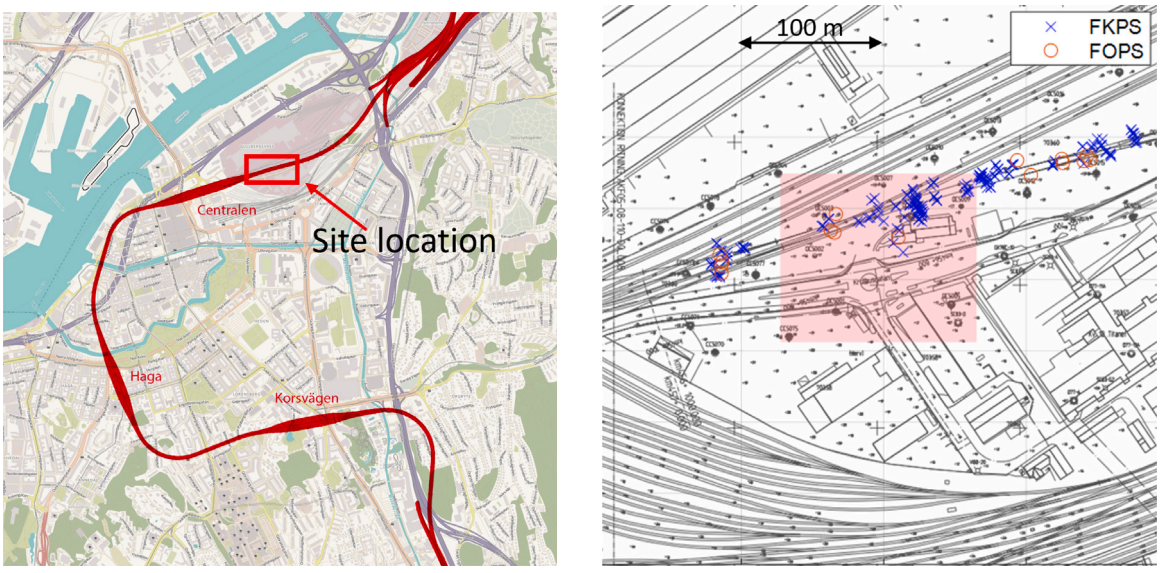

Fig. 1. (a) Site location: https://upload.wikimedia/Västlänken.org (b) Location FKPS and FOPS tests conducted with schematic of the cross-section of the excavation and column layout.

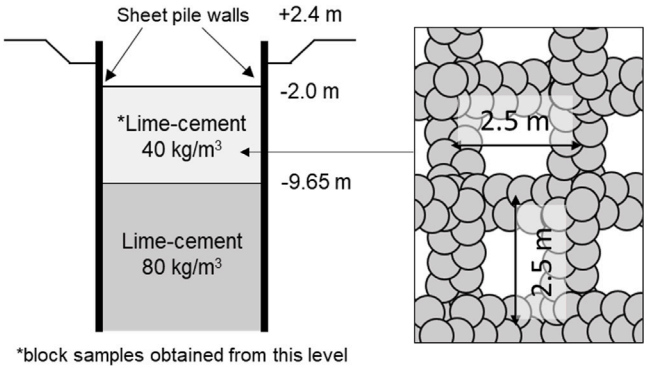

Fig. 2. Plan view of lime-cement column arrangement and cross-section of site.

time of sampling. The block samples were highly heterogeneous with weak zones of untreated clay and stiff cemented zones. Cylindrical samples (50 mm in diameter and 100 mm in height), and cubic samples (60 mm × 60 mm × 120 mm approximately) were cut from the block samples using a handheld saw.

3.2.2. Unconfined compression test

Unconfined compressive strength (UCS) tests were conducted on six samples as tabulated in Table 1. The tests utilised a GDS loading system with a 10 kN load cell to measure the axial load. In four of the tests, a pair of extensometers with a resolution of 1 μm were used to measure the local strains at the middle section of the samples. The unconfined compressive strength q_u and stiffness properties, including Young's modulus E, tangent modulus E_{tan}, secant modulus E_{sec}, and modulus at 50% peak unconfined compressive strength E_{50}, were derived from the UCS test results.

3.2.3. Digital image correlation

Two cubic samples of dimensions approximately 60 mm × 60 mm × 120 mm were tested in an uniaxial loading system with a stereoscopic digital image correlation (DIC) system, to identify strain localisation and non-uniform deformation due to material heterogeneity. The specifications of the samples are summarised in Table 2.

A MTS Series 300 frame with a 100 mm total stroke actuator and 100 kN maximum force capacity was used. The GOM DIC system consisted of two cameras with a resolution of 3000 × 4000 pixels facing one face of the cubic sample. Image data was captured at a rate of 6 frames per second. These images were then processed using stereo image correlation software (GOM Correlate), to extract the corrected image data for subsequent processing.

The strain distribution was computed from the corrected image data using the DIC scripts in SPAM (Software for the Practical Analysis of Materials) Python package [34]. Prior to the analyses, the images were binned to a size of 1500 × 2000 pixels. Furthermore, the intensity levels of the image data were pre-processed to obtain a uniform histogram for the image stack prior to further analyses. The displacement and strain analyses in SPAM were conducted on a rectangular spatial grid with a spacing of 30 pixels and used a half window size of 15 pixels.

The computed strains from the image data were used to obtain the local stiffness in the sample as function of the height. The specimen was divided into horizontal slices of 30 pixels in thickness, and the stiffness of each slice was thus approximated from the local average strain calculated from DIC and the average stress calculated from the load and updated area in each cross section. In this approximation, symmetry was assumed for calculating the average axial stress from the load cell readings.

3.2.4. X-ray computed tomography

The RX Solutions EasyTom150 X-ray tomograph at the 4D imaging lab at Lund University was used to acquire the three-dimensional scans of the samples. The X-ray source operated at a voltage of 80 kV with a current of 375 μA, and 2000 projections were used for the volumetric reconstruction of each sample. An additional filter of 0.35 mm copper sheet was added in front of the source to filter out low energy X-rays. The voxel size attained was 30 μm^3. Six cylindrical samples were analysed (see Table 3).

3.2.5. Image pre-processing

Pre-processing of the XCT image data was required to suppress the image noise and to accurately capture the variability in X-ray

Table 1
Testing programme for UCS tests.

Sample	Height (mm)	Diameter (mm)	Weight (kg)	Moisture content (%)	Loading rate (%/min)	Local axial measurement (y/n)
S7	103.5	53.46	342.8	62.63	0.1	y
S8	111.7	52.40	371.5	58.42	0.1	y
S9	106.8	47.30	289.3	65.40	0.01	y
S10	90.23	51.67	295.9	64.59	0.01	y
S11	92.42	52.19	300.0	65.56	0.1	n
S12	101.1	52.54	331.8	63.65	0.1	n

Table 2
Description of samples for unconfined compression test with DIC.

Sample	Height (mm)	Width 1 (mm)	Width 2 (mm)	Weight (kg)	Moisture content (%)	Loading rate (%/min)
S13	112.0	63.81	66.46	732.1	65.34	0.1
S14	119.9	60.61	60.44	669.8	64.32	0.01

Table 3
Summary of lime-cement mixed clay samples scanned with XCT.

Sample	Sample diameter (mm)	Sample height (mm)
S1	49.54	97.80
S2	49.54	97.06
S3	48.35	104.81
S4	49.10	91.07
S5	49.30	102.94
S6	48.15	103.07

attenuation of each specimen using auto-correlation of the image data. First, the data sets were binned (2 × 2 × 2 pixels averaged into 1 voxel) and each image slice, from a dataset of approximately 3500 slices, was cropped to 550 × 550 pixels (60 μm/pixel) to facilitate the analysis. The middle 1000 slices of the data set were considered, which corresponded to approximately 60 mm (Fig. 3).

The histogram of grey-scale intensities was normalised using the image processing package Fiji [35] to improve the contrast across the stack. The latter is permissible, as we are interested in the spatial variation and not the absolute values for the X-ray attenuation fields. Fig. 3(a) shows an example of a typical slice in the three-dimensional image obtained from the scan, and Fig. 3(b) shows the image after histogram normalisation. The parts in the image with higher grey-scale intensity correspond to regions of relatively higher X-ray attenuation (hence larger atomic number, material density), while the darker parts correspond to regions of relatively lower density. Therefore, the variation in grey-scale intensity level was used to estimate the variability in density of the specimen, where cemented clay corresponds to higher material density.

3.3. Estimation of SOF

Various methods are available to estimate the scale of fluctuation. This study adopts the simplest approach, which is to fit the theoretical correlation model (auto-correlation model) to the experimental correlation function [21,36–38]. The theoretical correlation model was assumed to have an exponential form:

$$R(\tau) = e^{\frac{-2\tau}{\theta}} \tag{2}$$

where $R(\tau)$ is the correlation coefficient between two points separated by a lag distance τ and θ is the scale of fluctuation. Other auto-correlation models have been employed in the geotechnical field [37,38]. However, Spry et al. [39] noted that no auto-correlation model is consistently better performing than the other functions. Eq. (2) was fitted only to the first part of the experimental correlation plot, to increase the reliability of the estimate of the scale of fluctuation [38].

3.3.1. SOF from field measurements

The range of depths used to determine the scale of fluctuation was selected based on the quality of the data recorded on-site. The FKPS probe that is axially penetrated into the column, is most accurate near the surface, where the probe deviates the least from the vertical alignment. Hence for the FKPS, data points in the range of 2 m to 8 m depth were selected. In contrast, the FOPS, which is a bottom up technique, provided the most complete dataset in the range of 10 m to 18 m depth.

3.3.2. SOF estimated from auto-correlation of image data

The scale of fluctuation was estimated from the variation in grey-scale intensity levels in the image data from the samples of lime-cement mixed clay, using auto-correlation of the two- and three-dimensional image data. The covariance of the images along each axis was computed using the function provided in SPAM [34]. The experimental correlation function was then computed by normalising the covariance values by the variance value. By fitting a theoretical auto-correlation function (Eq. (2)) to the experimental correlation coefficients obtained by this method, the SOF, along each axis, can be estimated based on the grey-scale intensity values of the image stack (Fig. 3). The variation in X-ray attenuation fields is not a direct measure of strength or stiffness of the sample, as it is most closely linked to the density of the material. For the samples tested, however, higher density areas are related to areas with a larger amount of cement, which has a higher X-ray attenuation than clay mineral. Thus, these areas are expected to have relatively higher strength and stiffness. Consequently, the SOF of X-ray attenuation fields represents the spatial variation in the mechanical properties of the material.

The theoretical auto-correlation function, shown in Eq. (2), was used to estimate the SOF along each axis. Axis 0 corresponds to the vertical direction (along the height of the cylindrical sample), while axes 1 and 2 correspond to orthogonal directions in each image slice. The same analysis was conducted for images of the front face of samples S13 and S14 prior to the application of a speckle (for subsequent DIC analyses) and loading.

4. Results and discussion

4.1. Unconfined compressive strength and stiffness from UCT

The unconfined compressive strength and stiffness obtained from the unconfined compression tests on cylindrical samples are summarised in Table 4. Figs. 4(a) and 4(b) show the variation of unconfined compressive strength q_u with axial strain ε and with average local axial strain ε_{local}, respectively. The range of q_u obtained was 1.03 MPa to 2.56 MPa, with a mean value of 1.96 MPa, standard deviation of 0.65 MPa and coefficient of variation (COV) of 0.33. The spread of values for the q_u prior to failure can be attributed to the inherent variability in the field mixed samples.

The Young's modulus E for the samples tested ranged from 199 MPa to 398 MPa. The variation in the E_{sec} and E_{50} values followed a similar range to the E values. The secant stiffness E_{sec} on average was seen to be 0.7–0.8 times E. In contrast, significant differences were observed between the values of E_{50} and E_{local}. The average local stiffness E_{local}, which is independent of bedding effects and stiffness of the

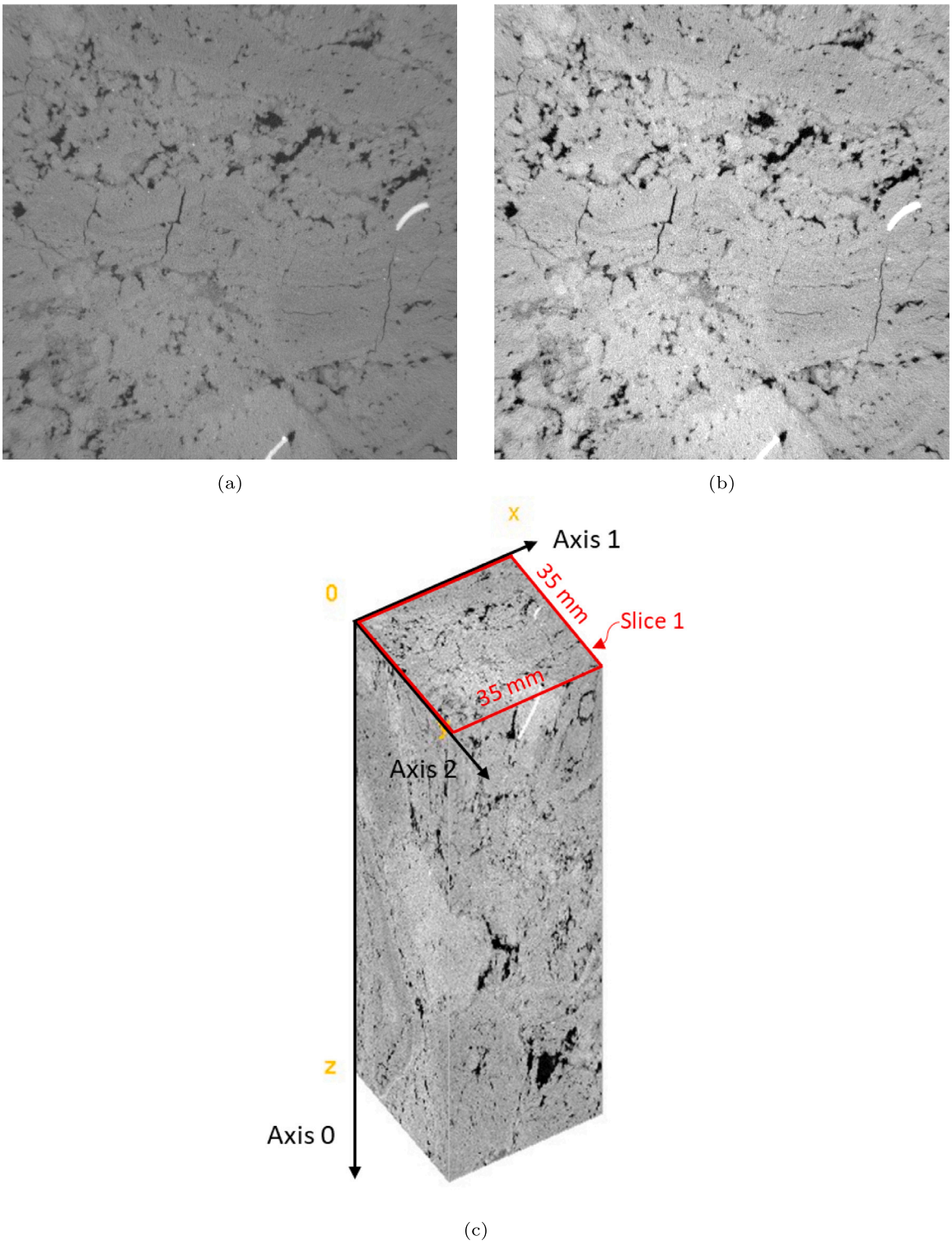

Fig. 3. (a) Image slice 1 of sample S2 in original grey scale and (b) after histogram normalisation. (c) Cropped 3D image stack from sample S2.

testing apparatus, was found to be on an average 6 times E. This is expected as local stiffness is more representative of the small-strain stiffness of the material. The local stiffness values obtained from the DIC measurements shown later corroborate this finding.

The E_{50} of the six samples tested is plotted against q_u in Fig. 5. Swedish design guidelines provides the empirical relationship $E = 13s_u^{1.6}$ or $E = 13(q_u/2)^{1.6}$, that relates shear strength of the lime-cement mixed soil to stiffness. However, this relation is unsuitable for this study as it is only applicable for $s_u < 150$ kPa. The samples tested in this study are approximately 1 year old and hence the shear strength far exceeds 150 kPa. Paniagua et al. [19] reported that for Norwegian clays improved with lime-cement with up to 54 days curing period and q_u ranging from 20 kPa to 450 kPa, the values of E_{50} vary between $50q_u$ and $800q_u$. In this study, E_{50} varies between $110q_u$ and $235q_u$, and the best-fit line was found at $133q_u$. A E_{50}/q_u ratio of 133 is also reasonably close to the range reported by Lee et al. [40] and Lorenzo and Bergado [41] for cement-clay mixed by jet-grouting method and deep mixing method. Due to the limited number of samples tested in

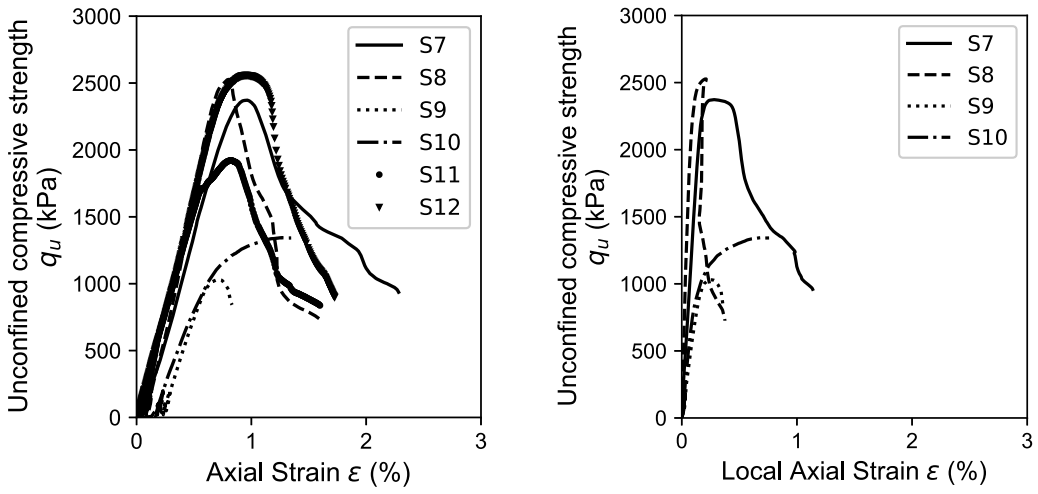

Fig. 4. Unconfined compressive strength q_u vs. (a) axial strain ε and (b) local axial strain ε_{local}.

Table 4
Strength and stiffness results from UCS.

Sample	q_u (MPa)	E (MPa)	E_{tan} (MPa)	E_{sec} (MPa)	E_{50} (MPa)	E_{local} (MPa)
S7	2.37	247.10	24.48	247.10	267.00	1424.36
S8	2.53	398.90	38.19	344.30	305.60	3122.30
S9	1.03	230.00	11.72	203.60	234.80	589.24
S10	1.34	199.70	7.67	112.50	211.30	1425.50
S11	1.92	305.90	6.70	235.40	312.70	–
S12	2.56	335.60	6.30	268.60	319.50	–

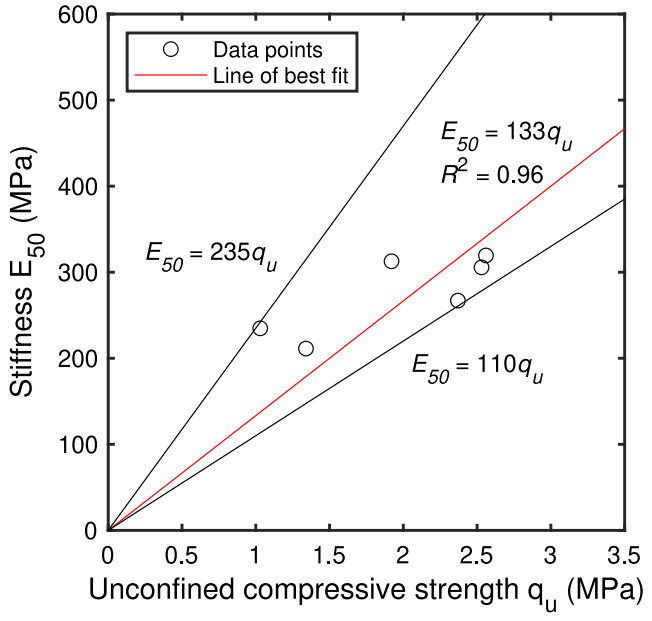

Fig. 5. Variation in stiffness with unconfined compressive strength.

this study, a more detailed relationship between strength and stiffness could not be identified. Nonetheless the linear relationships adopted from the literature provide some guidance on the relationship between E_{50} and q_u for lime-cement improved soft clay.

4.2. Image-based methods for estimating SOF

4.2.1. Stiffness variation from DIC

The global stiffness of samples S13 and S14, as determined from external Linear Variable Differential Transformer (LVDT) measurements, are 319 MPa and 229 MPa, respectively. The globally measured stiffness value does not give any additional information on the variability within the specimen, as it is expected that stiffness is non-uniform throughout the sample. Areas of cemented material and uncemented material can be observed by visual inspection. This spatial variation was further investigated using tests with simultaneous surface DIC.

Fig. 6 shows the vertical strain distribution obtained from DIC of the image data from the face of sample S13, for the loading stages indicated in Fig. 10(a). Negative strains correspond to compression and positive strains correspond to extension. A non-uniform distribution of strains with localisation on areas of uncemented clay can be observed, starting in the linear region (stages 1 to 3 in Fig. 10(a)), and becoming more pronounced after the peak stress was reached (stages 4 to 8 in Fig. 10(a)). Fig. 8 depicts the strain variation in the linear region with an adjusted scale to better visualise the non-uniform strain distribution and localisation. Figs. 7, 9 and 10(b) show the corresponding plots for sample S14.

The variation in local stiffness across the height of the samples S13 and S14, estimated from DIC strain measurements, is shown in Figs. 11(a) and 12(a). Only strain measurements in the linear regime (stages 1 to 3 in Fig. 10, corresponding to strains distributions shown in Figs. 8 and 9) were considered for the stiffness calculation. The strain field measurement had the highest accuracy in the middle portion of both cubic samples, due to end effects arising from dimensional tolerances of the manually sawed samples. For S13, this led to extension near the top of the sample, as seen from Fig. 6.

The local stiffness values obtained from DIC strain measurements are similar to the stiffness obtained from local strain measurements from the local transducers (Table 4), and similarly, are much larger than the global stiffness E (Table 4). Figs. 11(b) and 12(b) show the experimental and fitted correlation functions for the local stiffness variation along sample height, for S13 and S14 respectively, and the results are summarised in Table 5. Sample S13 which had a higher global stiffness, also had a smaller scale of fluctuation compared to S14, indicating that S13 had more variable stiffness along axis 0, as compared to S14.

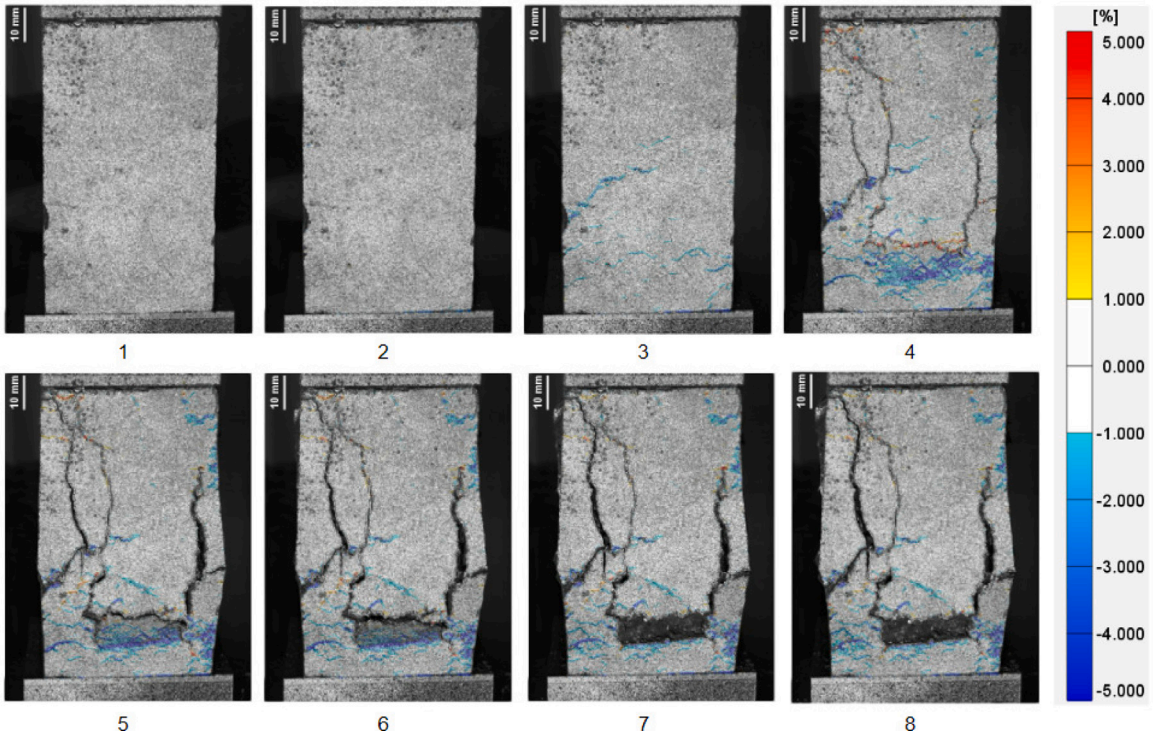

Fig. 6. Vertical strain field for sample S13.

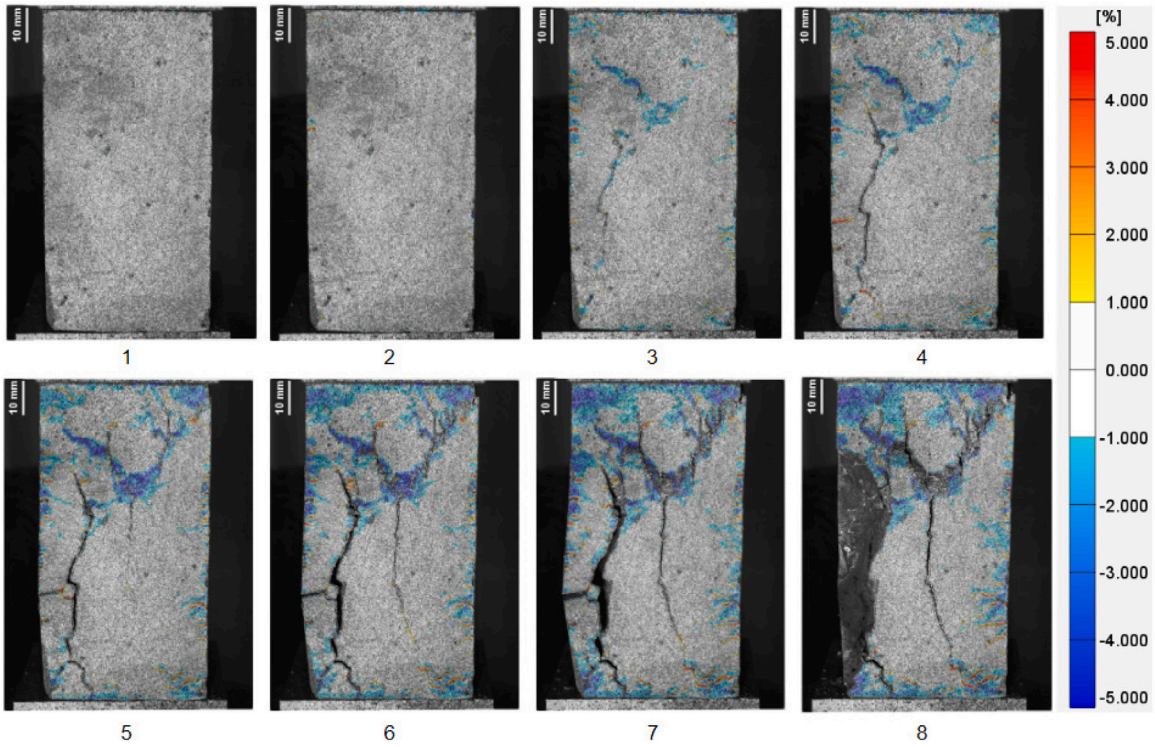

Fig. 7. Vertical strain field for sample S14.

4.2.2. Auto-correlation of image data

Fig. 13(a) shows the image of the front face of S13 taken with a digital camera before the sample was tested in the uniaxial loading frame. The scale of fluctuation, computed using the methodology discussed in Section 3.3.2, along axis 0 and axis 1 of the two-dimensional image, along with the fitted theoretical auto-correlation function, is shown in Figs. 13(b) and 13(c) respectively.

The SOF along axis 1 was estimated to be 2.1 mm for S13 and 6.8 mm for S14, which is smaller than the SOF estimated from the stiffness distribution obtained from DIC analysis (Table 5). Nevertheless, the

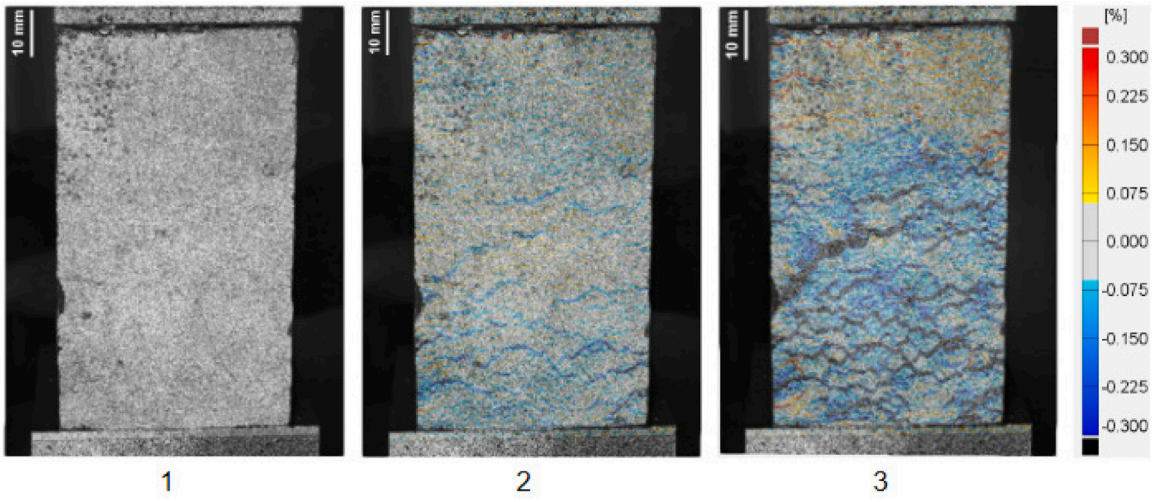

Fig. 8. Vertical strain field for sample S13 in the linear region.

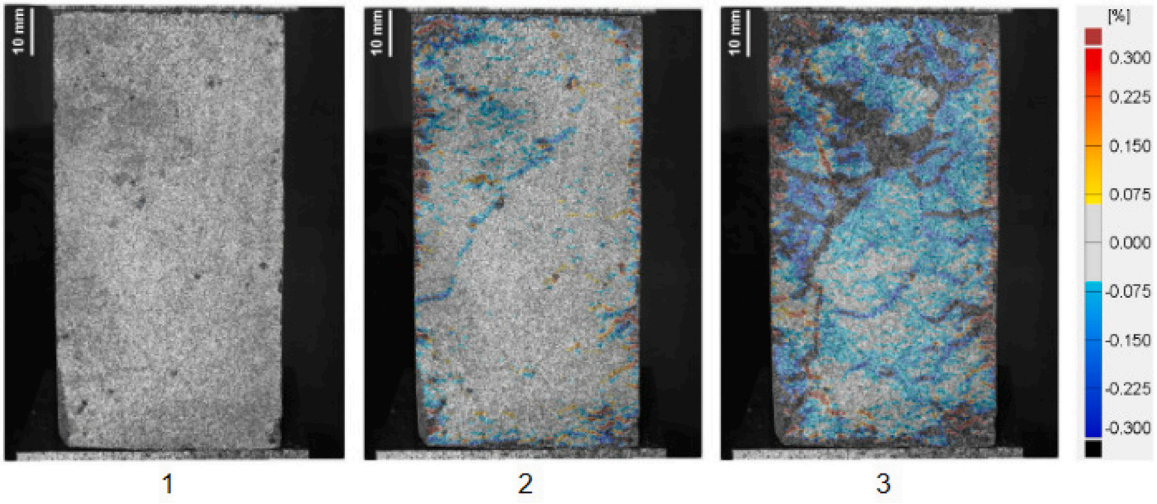

Fig. 9. Vertical strain field for sample S14 in the linear region.

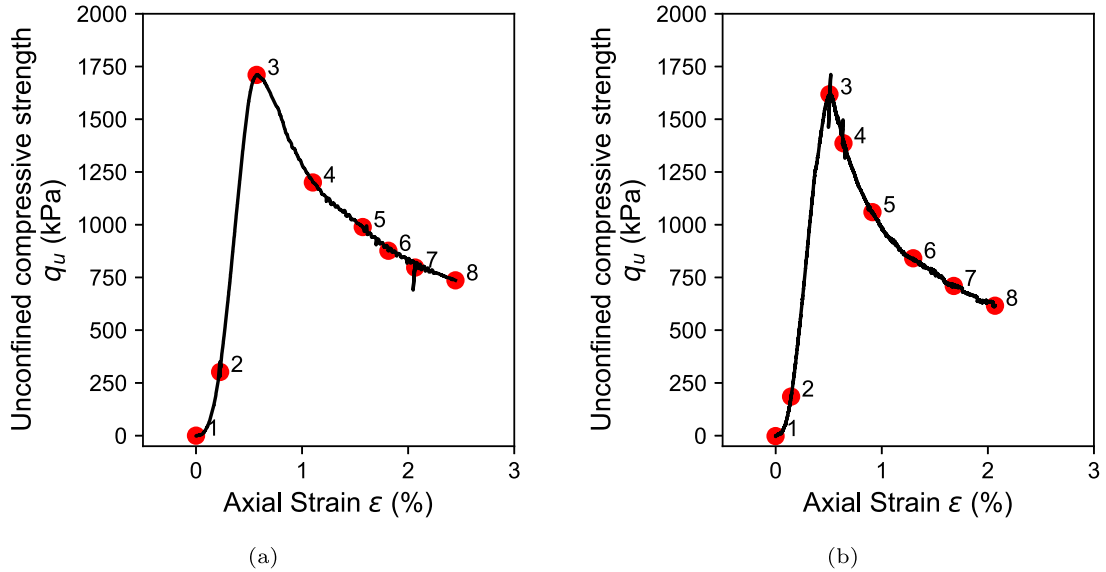

Fig. 10. Unconfined compressive strength q_u vs. Axial strain ε for (a) S13 and (b) S14.

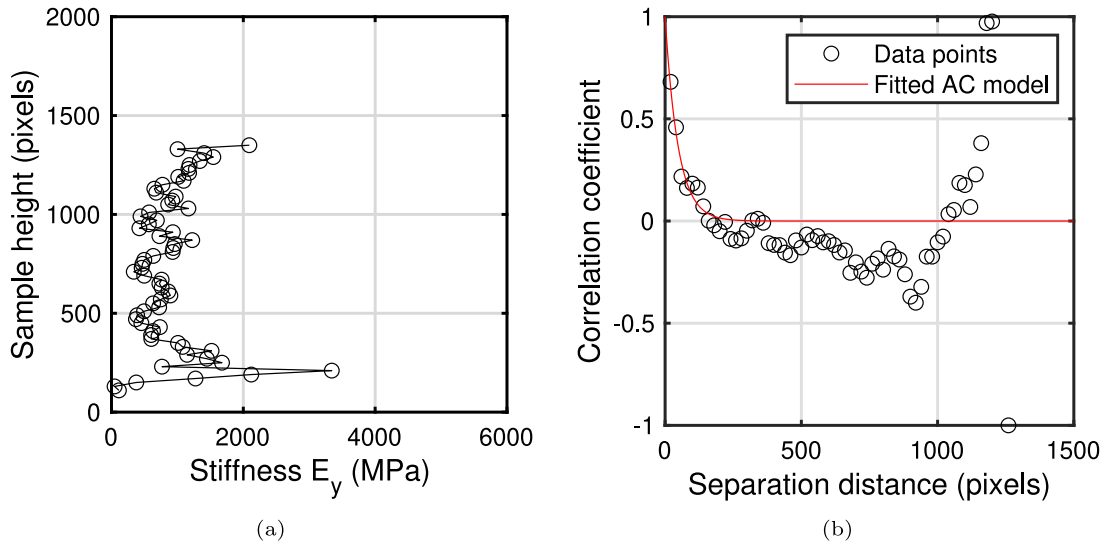

Fig. 11. (a) Stiffness variation with sample height and (b) experimental and fitted correlation function for stiffness along height of S13.

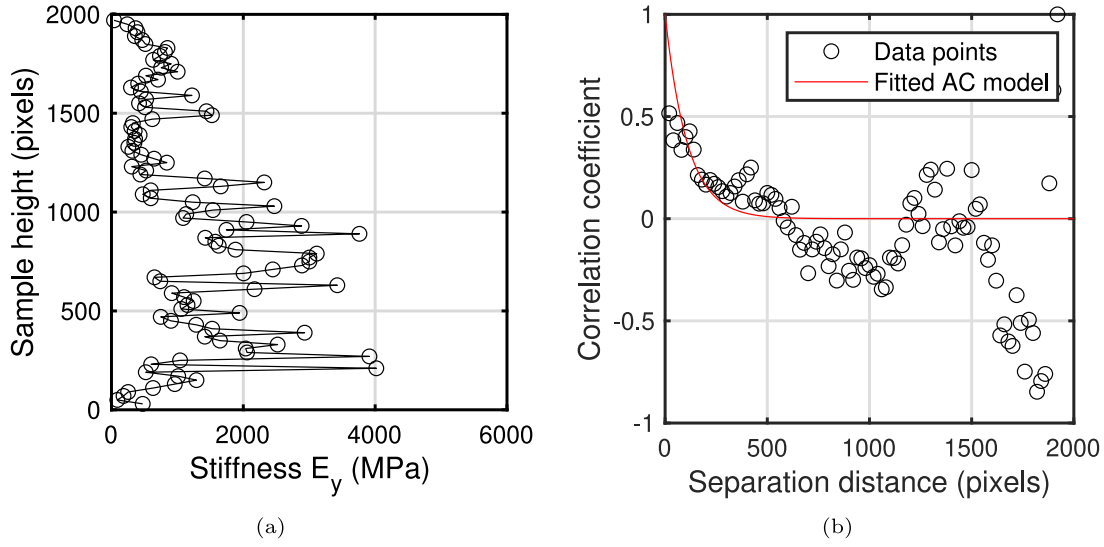

Fig. 12. (a) Stiffness variation with sample height and (b) experimental and fitted correlation function for stiffness along height of S14.

Table 5
Stiffness measurements from DIC.

Sample	E (MPa)	Average E_{local} (MPa)	Standard deviation E_{local} (MPa)	SOF_{axis0} (mm)
S13	319	974	670	5.4 (96 pixels)
S14	229	1194	937	13.0 (219 pixels)

same trend was observed that S13 which had the higher global stiffness, had a smaller scale of fluctuation along the vertical direction compared to S14. This corroborates the findings from the DIC measurements that S13 showed more variability (in the vertical direction) as compared to S14.

A possible explanation is that the auto-correlation of image data is more sensitive to the variations as compared to the DIC measurements as it considers all variation in grey-scale levels, which does not necessarily correlate to variation in stiffness. Furthermore, the DIC stiffness distribution was computed by taking average vertical strain across a slice (sub-window size of 30 pixels), resulting in some averaging effects of the stiffness computed. The size of the sub-window selected would affect the variation in stiffness captured. Using a sub-window size of 30 pixels, a reasonable estimate of the variation in stiffness with depth was captured, as seen from Figs. 11(a) and 12(a). The scale of fluctuation estimated from this analysis was 3.2 times and 7.3 times the sub-window size for S13 and S14 respectively. These values were smaller than a sample height of 2000 pixels, suggesting that the selected sub-window size was adequately small to accurately capture the stiffness variation along the sample height (Figs. 11(b) and 12(b)).

For S13, the SOF in both axes 1 and 2 were comparable, but S14 showed a higher SOF along axis 1 indicating the sample was less variable along axis 1 as compared to axis 2. The results are non-conclusive, as only two cubic samples were tested. Furthermore, information on the variability in the in plane direction (axis 0) cannot be determined from the two-dimensional image.

The image auto-correlation approach presented in the previous section was adopted for the three-dimensional XCT image stacks for six cylindrical samples. An example of the experimental correlation coefficient and fitted correlation function is shown in Fig. 14. The average value (for all six samples) of the SOF along axis 0, axis 1, and axis 2 are 1.08 mm, 1.46 mm, and 1.53 mm respectively. The estimated SOF for each sample is summarised in Table 6. The SOF along axis 0 is consistently smaller than the corresponding values along axis 1 and axis

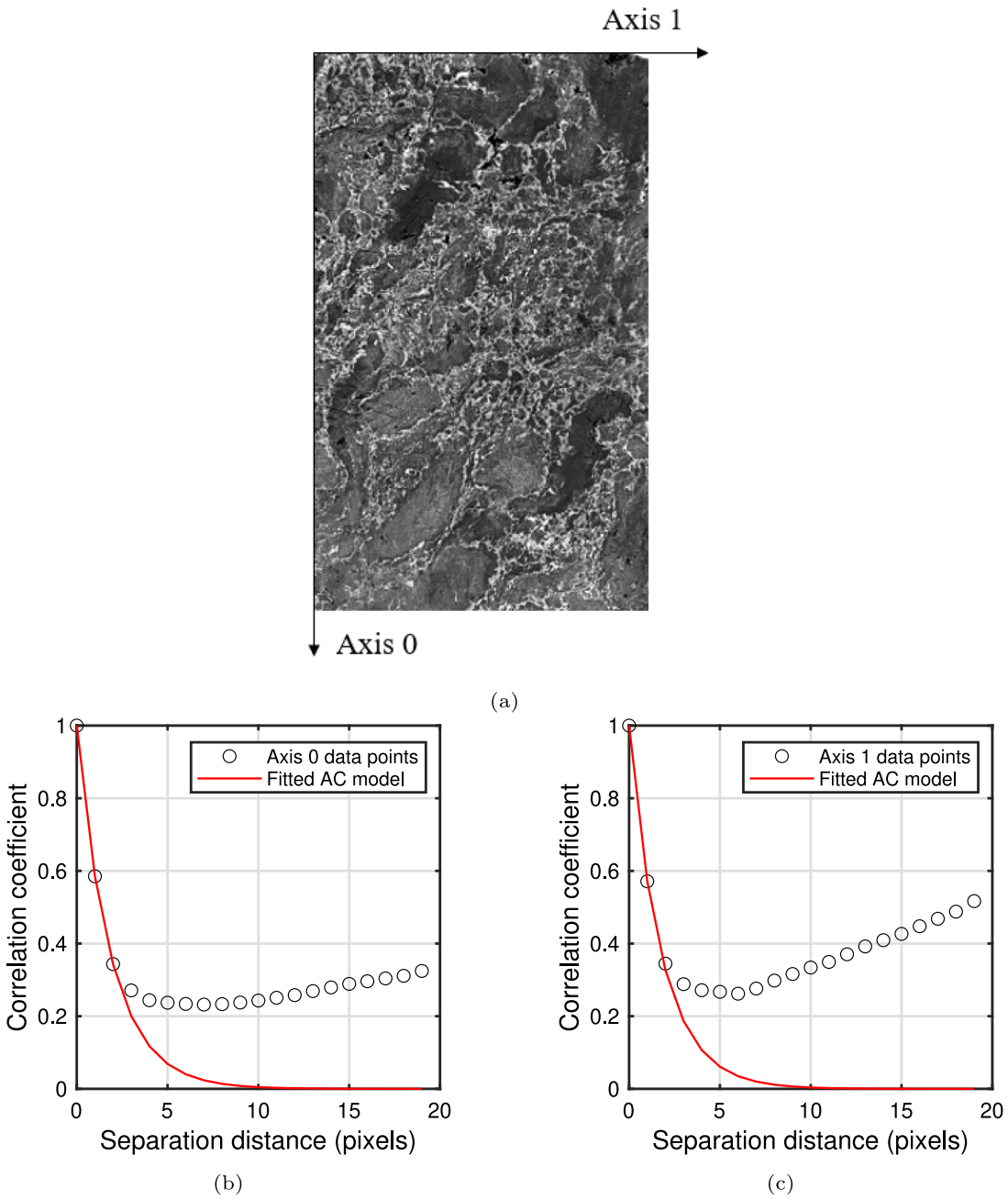

Fig. 13. (a) Front of S13, cropped to image size of 213 pixels × 386 pixels. (b) SOF along axis 0 and (c) along axis 1.

2, across all samples tested. This indicates that based on the variation in grey-scale intensity of the XCT image stack, the lime-cement samples are more variable in the vertical direction (along axis 0), than along the horizontal plane (along axis 1 and 2).

4.3. SOF from field test data

Fig. 15(a) shows the variation of shear strength with depth obtained from FKPS. Fig. 15(b) shows the corresponding plot for pull-out force obtained from FOPS. The pull-out force includes the friction on the wire as the probe is pulled through the column, which is different from the FKPS which uses local measures of force to push the probe into the column. The mean of both data sets is shown by the solid black line.

Beyond a depth of approximately 12 m, the raw FKPS data shows a general trend of decreasing shear strength with depth (Fig. 15(a)). It is expected that the shear strength increases with depth, which is seen in the FOPS data (Fig. 15(b)). This can be attributed to the errors associated with FKPS testing. As the probe is axially penetrated the lime-cement column from the ground surface downwards, there

Table 6
Scale of fluctuations estimated auto-correlation of image data.

Sample	SOF_{axis0} (mm)	SOF_{axis1} (mm)	SOF_{axis2} (mm)
S1	1.28	1.99	1.85
S2	0.79	0.96	1.50
S3	1.13	1.59	1.40
S4	1.30	1.75	1.77
S5	1.03	1.30	1.35
S6	0.95	1.20	1.31
S13	–	2.1	2.1
S14	–	6.3	3.8

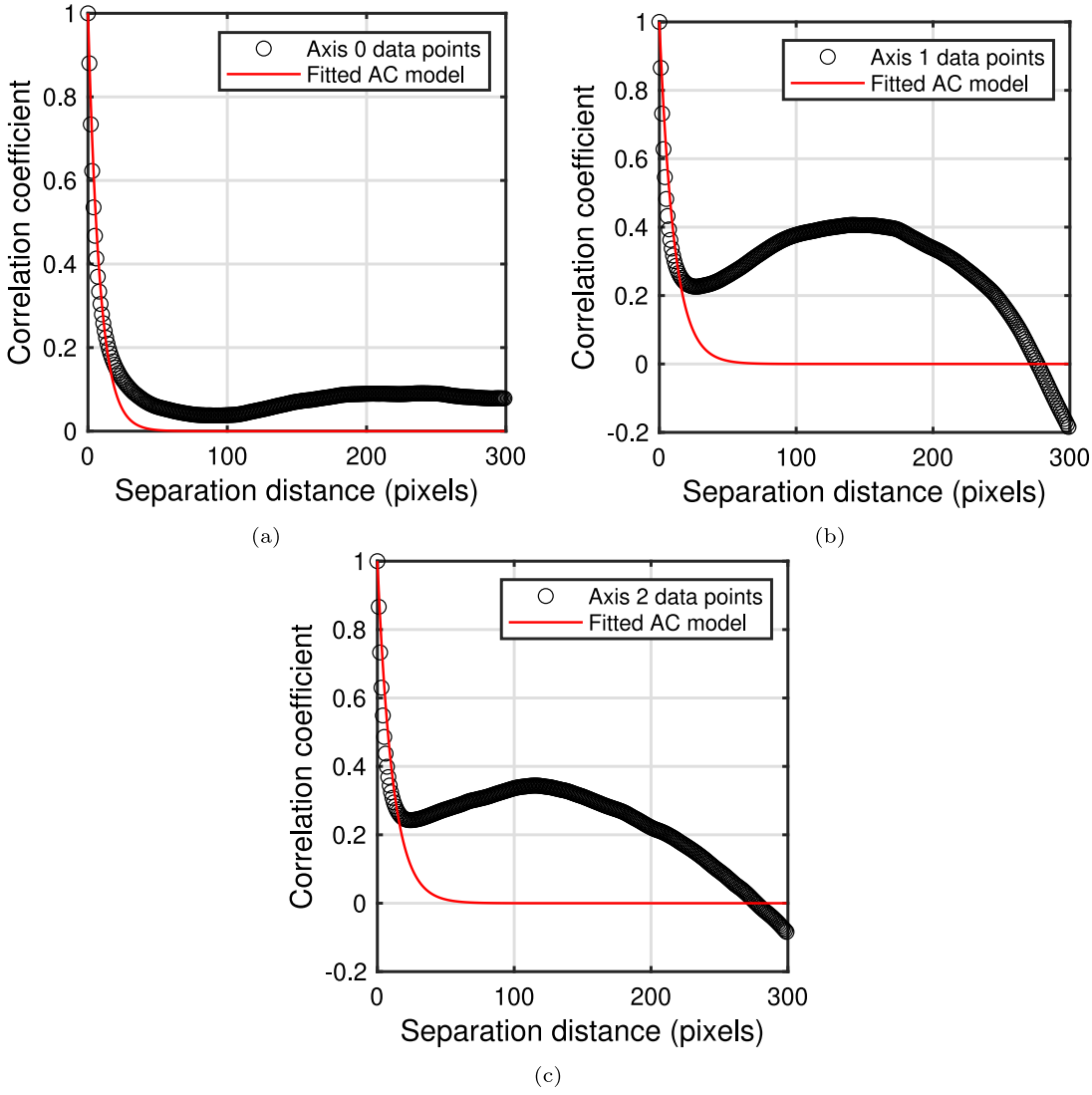

Fig. 14. Example of calculated correlation coefficient and fitted auto-correlation function along (a) axis 0 (b) axis 1, and (c) axis 2 for sample S6.

is a tendency for the probe to deviate from alignment into the softer surrounding soil as it encounters increasing stiff material at greater depths. The FOPS test which starts at the base of the column is thus more reliable strength measurement at larger depths.

4.3.1. Distribution

Fig. 16 shows the distribution of the shear strength and pull-out force from the column tests. The mean value of the shear strength is 194 kPa, and the standard deviation and COV were 116 kPa and 0.60, respectively. The mean value of the pull-out force is 27.2 kN, and the standard deviation and COV were 23.2 kN and 0.86.

4.3.2. SOF_y

Fig. 17(a) shows the distribution of the scale of fluctuation in the vertical direction SOF_y determined from the FKPS data. The range of SOF_y values estimated from FKPS was 0.4 m to 3.5 m and the mean value was 1.4 m. Fig. 17(b) shows the corresponding results from the FOPS data. The range of SOF_y values estimated from FOPS was 0.3 m to 2.0 m and the mean value was 0.9 m. The results indicate that FOPS might have an inherently larger measurement error, as it has a smaller mean SOF_y value as compared to FKPS. Notwithstanding this, FOPS is superior for larger depths which cannot be reliably assessd by FKPS. The SOF_y of the lime-cement columns is 3 to 4 times smaller than that of the original clay deposit (as derived from cone penetration test (CPT) data prior to construction).

The values for SOF_y obtained in this study are summarised in Table 7, together with values reported in literature. The mean values and the range of SOF_y from this study are slightly larger than those reported in the literature which indicated that the lime-cement columns tested in this study are relatively less variable than those of previous studies [30,31]. This could possibly be attributed to differences in site conditions and also the larger data set considered and longer column lengths tested in the current study.

4.3.3. SOF_x

The scale of fluctuation in the horizontal direction (SOF_x) was evaluated at 0.5 m intervals for both the FKPS and FOPS data sets. At each 0.5 m depth interval, data points from all testing locations were grouped by separation distance to compute the correlation coefficients and fit the theoretical correlation model.

Fig. 18(a) shows the distribution of the scale of fluctuation in the horizontal direction SOF_x determined from the FKPS data. The range of SOF_x values estimated from FKPS was 0.4 m to 4.3 m and the mean value was 1.6 m. Fig. 18(b) shows the corresponding results from the FOPS data. The range of SOF_x values estimated from FOPS was 4.0 m to 11.4 m and the mean value was 9.1 m. Figs. 19(a) and 19(b) show the distribution of SOF_x with depth.

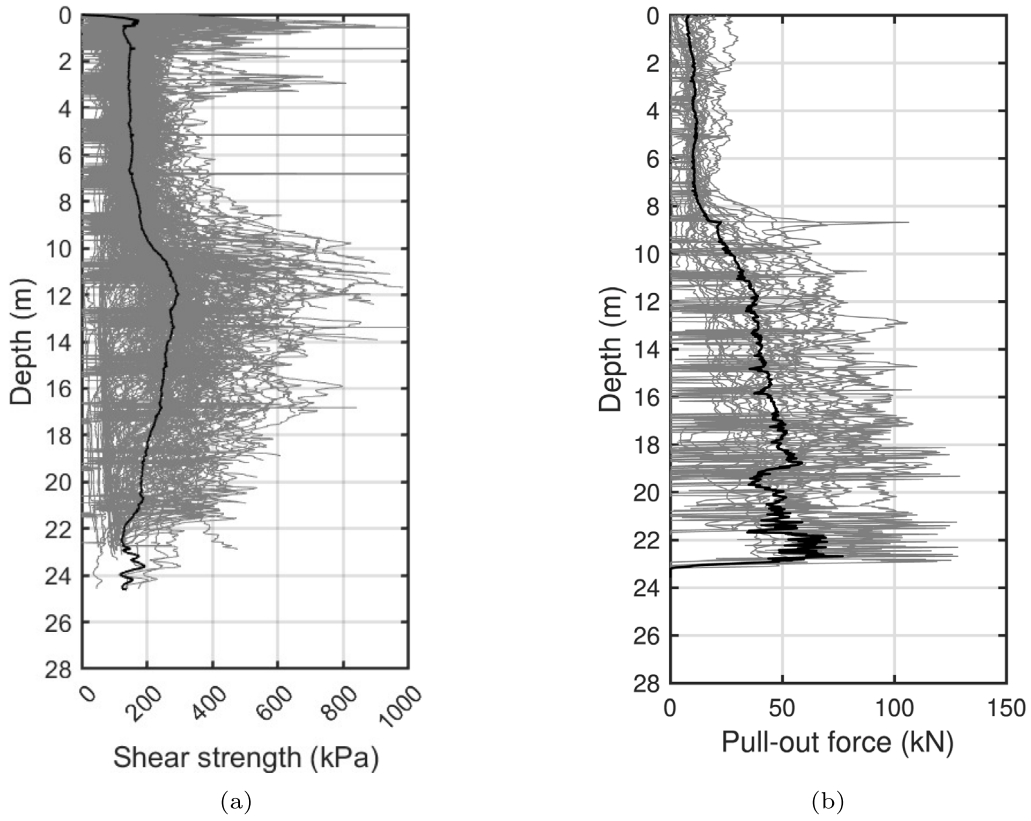

Fig. 15. (a) Variation of shear strength with depth of 202 FKPS tests. (b) Variation of pull-out force with depth of 29 F0PS tests.

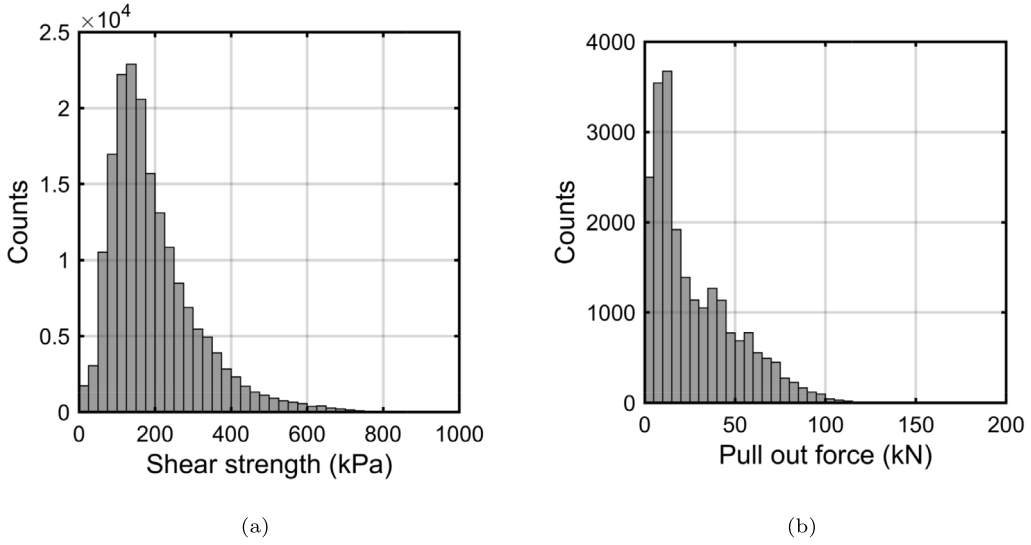

Fig. 16. Histogram distributions of (a) shear strength and (b) pull-out force obtained from FKPS and FOPS data, respectively.

While the range of SOF_x estimated from FKPS data is similar to the values reported in the literature [30,31], the range of SOF_x estimated from FOPS data was significantly larger. It would be incorrect to assume based on this result that the lime-cement columns have a low degree of variability. This is more likely due to limitations in the distribution of testing locations. The horizontal separation distances between the test locations have a significant influence on the SOF_x estimated. The testing locations of the FOPS data are few (29 locations) and irregularly spaced and clustered around certain parts of the site (Fig. 1(b)). As a result, majority of the horizontal separation distances between sampling points was approximately 3.0 m or 13.0 m to 17.0 m for the FOPS data set. This resulted in few and scattered data points in the correlation coefficient versus separation distance plot which consequently leads to poor fitting of the auto-correlation model. Thus, it is difficult to estimate with large accuracy a value of SOF_x that is smaller than the range of horizontal separation distances of the data set. The number of test locations from FKPS (202 locations) was significantly larger than that of FOPS, which resulted in less scatter and

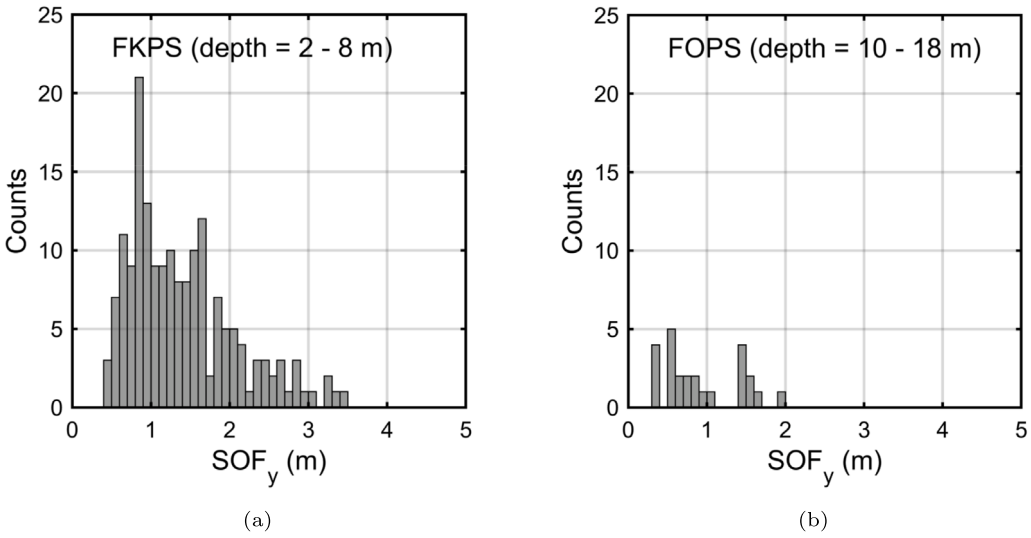

Fig. 17. SOF$_y$ from (a) 2 m to 8 m depth estimated from FKPS data sets and (b) 10 m to 18 m depth estimated from FOPS data sets.

Table 7
Summary of values for the scale of fluctuation in lime-cement columns from literature.

Reference	Test site	Depth of testing	Test Method	SOF_y (m)	SOF_x (m)
Larsson et al. [29]	Håby Strängnäs	1.9 m or 2.3 m	Hand operated penetrometer	–	<0.15 (radial) <0.35 (orthogonal)
Al-Naqshabandy et al. [42]	Lidatorp	0 m to 8 m	CPT sounding	0.2 m to 0.7 m	2 m to 3 m
Bergman et al. [31]	Kista Lidingö	0 m to 6 m	CPT sounding KPS sounding	0.11 m to 0.77 m	3 m to 4 m
This study	Gothenburg (Centralen)	2 m to 8 m	FKPS	0.4 m to 3.5 m 1.4 (average)	0.4 m to 4.3 m 1.6 (average)
		10 m to 18 m	FOPS	0.3 m to 2.0 m 0.9 (average)	4.0 m to 11.4 m 9.1 (average)

relatively better fit of the correlation model. However, the distribution of the locations is irregular and not densely spaced with majority of the separation distances in the range of 3 m to 15 m. For a reliable estimate of SOF$_x$, a densely spaced array of test locations with regular intervals of separation distances should be adopted [29,31,43].

Moreover, it is important to note that the range of SOF$_x$ estimated for the site is larger than the array spacing of the lime-cement columns (Fig. 1(b)), and it would be incorrect to assume that the entire site is largely uniform in the horizontal direction based on SOF$_x$ values alone as there still are pockets of uncemented soil between the lime-cement columns. Instead, the SOF$_x$ is more of an indicator of the similarity between the lime-cement columns that are located within a horizontal separation distance approximately equal to SOF$_x$. Nevertheless, the SOF$_x$ values from FKPS is similar to that of Al-Naqshabandy and Larsson [30] and Bergman et al. [31] and provides some guiding values on the degree of horizontal spatial variability to be expected in lime-cement columns.

5. Conclusions

The strength and stiffness of lime-cement mixed clay is spatially variable. Hence, the characterisation of the extent of spatial variability of strength and stiffness is essential to optimise the performance of lime-cement columns. This paper presents an integrated approach to characterise the spatial variability in strength and stiffness of samples from lime-cement columns in natural sensitive clay, from the Centralen project site in Gothenburg, Sweden. The spatial variability is characterised at both the laboratory and field scale, using field-mixed samples and quality control data obtained from an excavation stabilised with lime-cement columns.

At the laboratory scale, stiffness and strength of the lime-cement mixed clay was obtained from unconfined compression tests, and E_{50} of the 1-year samples vary between $220q_u$ and $470q_u$. The spatial variability in stiffness was estimated using unconfined compression tests coupled with DIC analysis, which was effective in capturing the non-homogeneous strain distributions across the face of cubic samples, indicating the inherent variability of stiffness within the specimen. A novel image-based approach was adopted to characterise the scale of fluctuation in a specimen from the auto-correlation of grey-scale intensity of two and three-dimensional images. Grey-scale intensity is not a direct measure of strength or stiffness of the sample but the variation in grey-scale intensity is representative of the spatial variation in mechanical properties. This provides valuable information on heterogeneity of the specimen, especially for the three-dimensional image data from X-ray Computed Tomography. At the field scale, the scale of fluctuation in both the vertical and horizontal directions was estimated from field column penetration tests and reverse column penetration tests on 1 to 10 day old columns.

The key finding of this work is that different magnitudes of scales of fluctuations exist for the field mixed lime-cement improved clay under laboratory scale and field scale testing. This concept which was highlighted by Larsson et al. [29] states that the spatial variability of a parameter is connected to a certain length scale, and various

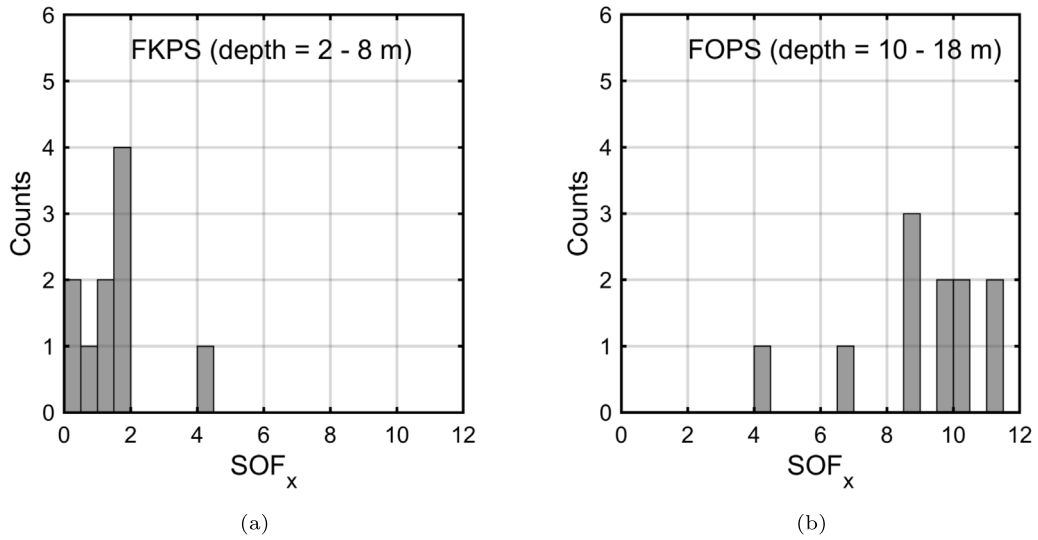

Fig. 18. SOF$_x$ from (a) 2 m to 8 m depth estimated from FKPS data sets and (b) 10 m to 18 m depth estimated from FOPS data sets.

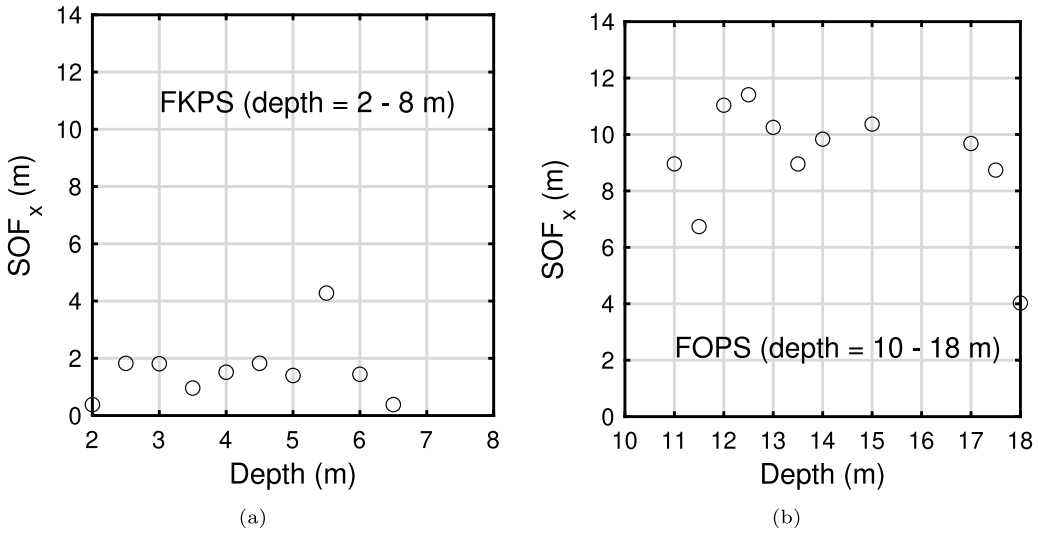

Fig. 19. SOF$_x$ vs. depth at (a) 2 m to 8 m depth estimated from FKPS data sets and (b) 10 m to 18 m depth estimated from FOPS data sets.

parameters influence at different scales. Consequently, it is important to determine the correlation structure related to the relevant scale of scrutiny. Work by Liu et al. [43] showed that if the sampling region is of a similar size to the column diameter, the measured scale of fluctuation reflects that of the intra-column variability. As the sampling region increases, the measured scale of fluctuation also increases. This explains the wide range of scales of fluctuations reported in this study in the laboratory scale and the field scale. The scale of fluctuation at the laboratory scale is very much smaller than that of the field scale, and likely represents the variation within one measurement interval or smaller of the field column penetration tests. The laboratory scale of fluctuation is expected to relate more to the element test level performance of the material. In contrast, the scale of fluctuation at the field scale is related to the global performance of the geotechnical structure.

Due to the limited samples available from the field, a comprehensive systematic study on the relationship between variability in strength and stiffness at the field and laboratory scale could not be explored more deeply. However, the results serve to highlight the ever present problem of inherent variability in lime-cement mixed soils and challenges to accurately characterise this variability. Thus, further work is required to relate scale of fluctuation of strength to that of stiffness, and to link scale of fluctuation at laboratory scale with that at field scale for material of the same age.

CRediT authorship contribution statement

Dawn Yun-Cheng Wong: Writing – review & editing, Writing – original draft, Supervision, Methodology, Investigation, Formal analysis, Data curation, Conceptualization. **Vijayshree Sadasivan:** Writing – review & editing, Methodology, Investigation, Formal analysis,

Data curation. **Jonatan Isaksson:** Writing – review & editing, Visualization, Resources, Investigation, Conceptualization. **Anders Karlsson:** Resources, Methodology, Data curation. **Jelke Dijkstra:** Writing – review & editing, Writing – original draft, Supervision, Software, Methodology, Investigation, Conceptualization.

Declaration of competing interest

The authors declare that they have no known competing financial interests or personal relationships that could have appeared to influence the work reported in this paper.

Data availability

Data will be made available on request.

Acknowledgements

This work is done as part of Chalmers Centre of Excellence in Railway Mechanics and is funded by Formas, Sweden (Research Council for sustainable Development, Grant 2021-01340) and Swedish Transport Administration, Sweden (Grant TRV 2021/26336) via BIG (Better Interaction in Geotechnics). The authors would also like to thank the West Link Project in Gothenburg, NCC Sverige AB, and the Swedish Transport Administration for making the field data available for this project.

References

[1] A. Porbaha, State of the art in deep mixing technology: part I. Basic concepts and overview, Proc. Inst. Civ. Eng. Ground Improv. 2 (2) (1998) 81–92, http://dx.doi.org/10.1680/gi.1998.020204.
[2] M. Terashi, The state of practice in deep mixing methods, in: Grouting and Ground Treatment, American Society of Civil Engineers, 2003, pp. 25–49.
[3] B. Broms, Lime and lime/cement columns, Ground Improv. 2 (2004) 252–330.
[4] Trafikverket, Trafikverkets Tekniska råd för Geokonstruktioner-TR Geo 13, Standard, Trafikverket, Sweden, SE, 2016.
[5] M. Topolnicki, In situ soil mixing, Ground Improv. 2 (2004) 331–428.
[6] S. Larsson, M. Dahlström, B. Nilsson, A complementary field study on the uniformity of lime-cement columns for deep mixing, Ground Improv. 9 (2) (2005) 67–77.
[7] F. Bell, Lime stabilization of clay minerals and soils, Eng. Geol. 42 (4) (1996) 223–237.
[8] M.D. Liu, B. Indraratna, S. Horpibulsuk, J. Suebsuk, Variations in strength of lime-treated soft clays, Proc. Inst. Civ. Eng. Ground Improv. 165 (4) (2012) 217–223.
[9] B.K. Fiskvik Bache, P. Wiersholm, P. Paniagua, A. Emdal, Effect of temperature on the strength of lime–cement stabilized norwegian clays, J. Geotech. Geoenviron. Eng. 148 (3) (2022) 04021198.
[10] S. Larsson, M. Dahlström, B. Nilsson, Uniformity of lime-cement columns for deep mixing: a field study, Proc. Inst. Civ. Eng. Ground Improv. 9 (1) (2005) 1–15.
[11] H. Åhnberg, S.-E. Johansson, H. Pihl, T. Carlsson, Stabilising effects of different binders in some Swedish soils, Proc. Inst. Civ. Eng. Ground Improv. 7 (1) (2003) 9–23.
[12] R. Ignat, S. Baker, M. Holmén, S. Larsson, Triaxial extension and tension tests on lime-cement-improved clay, Soils Found. 59 (5) (2019) 1399–1416.
[13] S. Larsson, The mixing process at the dry jet mixing method, in: International Conference on Dry Mix Methods for Deep Soil Stabilization, Stockholm, Balkema, 1999, pp. 339–346.
[14] K.-K. Phoon, F.H. Kulhawy, Characterization of geotechnical variability, Can. Geotech. J. 36 (4) (1999) 612–624.
[15] S. Horpibulsuk, R. Rachan, A. Suddeepong, A. Chinkulkijniwat, Strength development in cement admixed Bangkok clay: laboratory and field investigations, Soils Found. 51 (2) (2011) 239–251.
[16] S. Horpibulsuk, N. Miura, H. Koga, T. Nagaraj, Analysis of strength development in deep mixing: a field study, Proc. Inst. Civ. Eng. Ground Improv. 8 (2) (2004) 59–68.
[17] R.S. Madhyannapu, A.J. Puppala, S. Nazarian, D. Yuan, Quality assessment and quality control of deep soil mixing construction for stabilizing expansive subsoils, J. Geotech. Geoenviron. Eng. 136 (1) (2010) 119–128.
[18] A.J. Puppala, V. Bhadriraju, R.S. Madhyannapu, S. Nazarian, R. Williammee, Small strain shear moduli of lime-cement treated expansive clays, in: Geomechanics II: Testing, Modeling, and Simulation, American Society of Civil Engineers, 2006, pp. 58–70.
[19] P. Paniagua, B.r.K. Bache, K. Karlsrud, A.K. Lund, Strength and stiffness of laboratory-mixed specimens of stabilised norwegian clays, Proc. Inst. Civ. Eng. Ground Improv. 175 (2) (2022) 150–163.
[20] B.Z. Coelho, J. Nuttall, A. Noordam, J. Dijkstra, The impact of soil variability on uncertainty in predictions of induced vibrations, Soil Dyn. Earthq. Eng. 169 (2023) 107855.
[21] E. Vanmarcke, Probabalistic modeling of soil profiles, J. Geotech. Eng. Div. 103 (11) (1977) 1227–1246, http://dx.doi.org/10.1061/AJGEB6.0000517.
[22] G.B. Baecher, J.T. Christian, Reliability and Statistics in Geotechnical Engineering, John Wiley & Sons, 2005.
[23] G.A. Fenton, D.V. Griffiths, et al., Risk Assessment in Geotechnical Engineering, vol. 461, John Wiley & Sons New York, 2008.
[24] M. Lloret-Cabot, G.A. Fenton, M.A. Hicks, On the estimation of scale of fluctuation in geostatistics, Georisk 8 (2) (2014) 129–140.
[25] K. Kasama, A.J. Whittle, K. Zen, Effect of spatial variability on the bearing capacity of cement-treated ground, Soils Found. 52 (4) (2012) 600–619.
[26] T. Namikawa, J. Koseki, Effects of spatial correlation on the compression behavior of a cement-treated column, J. Geotech. Geoenviron. Eng. 139 (8) (2013) 1346–1359.
[27] J. Chen, F. Lee, C. Ng, Statistical analysis for strength variation of deep mixing columns in Singapore, in: Geo-Frontiers 2011: Advances in Geotechnical Engineering, 2011, pp. 576–584.
[28] Y. Liu, Y. Jiang, H. Xiao, F. Lee, Determination of representative strength of deep cement-mixed clay from core strength data, Géotechnique 67 (4) (2017) 350–364.
[29] S. Larsson, H. Stille, L. Olsson, On horizontal variability in lime-cement columns in deep mixing, Géotechnique 55 (1) (2005) 33–44.
[30] M.S. Al-Naqshabandy, S. Larsson, Effect of uncertainties of improved soil shear strength on the reliability of embankments, J. Geotech. Geoenviron. Eng. 139 (4) (2013) 619–632.
[31] N. Bergman, M.S. Al-Naqshabandy, S. Larsson, Variability of strength and deformation properties in lime-cement columns evaluated from CPT and KPS measurements, Georisk 7 (1) (2013) 21–36.
[32] S. Bozkurt, A. Abed, M. Karstunen, Finite element analysis for a deep excavation in soft clay supported by lime-cement columns, Comput. Geotech. 162 (2023) 105687.
[33] Trafikverket, Fullskaleförsök DDM (Dry Deep Mixing) i Passivzon, Delprojekt E02 Centralen, Västlänken, Technical Report, Trafikverket, Sweden, SE, 2018.
[34] O. Stamati, E. Andò, E. Roubin, R. Cailletaud, M. Wiebicke, G. Pinzon, C. Couture, R.C. Hurley, R. Caulk, D. Caillerie, et al., Spam: software for practical analysis of materials, J. Open Source Softw. 5 (51) (2020) 2286.
[35] J. Schindelin, I. Arganda-Carreras, E. Frise, V. Kaynig, M. Longair, T. Pietzsch, S. Preibisch, C. Rueden, S. Saalfeld, B. Schmid, et al., Fiji: an open-source platform for biological-image analysis, Nat. Methods 9 (7) (2012) 676–682.
[36] G.A. Fenton, Estimation for stochastic soil models, J. Geotech. Geoenviron. Eng. 125 (6) (1999) 470–485, http://dx.doi.org/10.1061/(ASCE)1090-0241(1999)125:6(470).
[37] E. Vanmarcke, Random Fields: Analysis and Synthesis, Cambridge, 1983.
[38] M. Uzielli, G. Vannucchi, K. Phoon, Random field characterisation of stress-normalised cone penetration testing parameters, Geotechnique 55 (1) (2005) 3–20.
[39] M. Spry, F. Kulhawy, M. Grigoriu, E.P.R. Institute, C.U.G.E. Group, Reliability-based foundation design for transmission line structures: Geotechnical site characterization strategy, in: Reliability-based Foundation Design for Transmission Line Structures: Final Report, The Institute, 1988, URL https://books.google.se/books?id=FLeLxgEACAAJ.
[40] F.-H. Lee, Y. Lee, S.-H. Chew, K.-Y. Yong, Strength and modulus of marine clay-cement mixes, J. Geotech. Geoenviron. Eng. 131 (2) (2005) 178–186.
[41] G.A. Lorenzo, D.T. Bergado, Fundamental characteristics of cement-admixed clay in deep mixing, J. Mater. Civ. Eng. 18 (2) (2006) 161–174.
[42] M.S. Al-Naqshabandy, N. Bergman, S. Larsson, Strength variability in lime-cement columns based on cone penetration test data, Proc. Inst. Civ. Eng. Ground Improv. 165 (1) (2012) 15–30.
[43] Y. Liu, L. He, Y. Jiang, M. Sun, E. Chen, F.-H. Lee, Effect of in situ water content variation on the spatial variation of strength of deep cement-mixed clay, Géotechnique 69 (5) (2019) 391–405.